Available online at www.sciencedirect.com
SCIENCE DIRECT®
Optics Communications 255 (2005) 338–348
OPTICS COMMUNICATIONS
www.elsevier.com/locate/optcom

Light transmission through a subwavelength hole

Evgeny Popov [a,*], Michel Nevière [a], Philippe Boyer [a], Nicolas Bonod [b]

[a] Institut Fresnel, Case 161, Unité Mixte de Recherche Associée au Centre National de la Recherche Scientifique (UMR 6133), Université de Provence, Faculté des Sciences et Techniques de St. Jérôme, Avenue Escadrille Normandie-Niémen, 13397 Marseille Cedex 20, France

[b] Commissariat à l'Energie Atomique, Centre d'Etudes Scientifiques et Techniques d'Aquitaine, BP No. 2, 33114 Le Barp, France

Received 7 April 2005; received in revised form 1 June 2005; accepted 3 June 2005

Abstract

We use a recently developed electromagnetic theory to get some insight of the physics that governs the extraordinary transmission of light by a hole pierced in a metallic screen. When the film thickness increases, a comparison is made between the decay of the total field and the decay of the field of the evanescent mode in the corresponding infinite hollow metallic waveguide. The decay behavior and the comparison between their field maps demonstrates that the transmission through the hole is determined by this guided mode. The near field maps below the hole shows small oscillations around a decaying mean value, when the observation points moves away from the hole ridge. The study of the plasmon excited at the bottom interface of the screen allows interpreting all the fine phenomena in terms of simple concepts.

Keywords: Single aperture; Surface plasmon; Evanescent modes; Enhanced transmission

1. Introduction

Despite the great amount of theoretical work published since the discovery of the extraordinary light transmission by subwavelength hole arrays [1], the physics of the process still remains not fully understood. Concerning periodic arrays, the key role of surface plasmons has been invoked from the very beginning [2–5]. The plasmon excitation at bottom interface was shown to occur thanks to a special channel [6,7] provided by periodic hole arrays. Then the coupling between the plasmons excited at both interfaces was shown both by experiments [8] and theory [9,10] to increase again the transmission. It was even found that such an extraordinary transmission could be obtained with modulated films without holes [11–13], provided they are thin enough to allow a coupling between the plasmons at the top and bottom interface. All the theoretical studies took advantage of the

* Corresponding author.
E-mail address: e.popov@fresnel.fr (E. Popov).

0030-4018/$ - see front matter
doi:10.1016/j.optcom.2005.06.010

bi-periodicity of the device to express the field components in terms of Fourier series.

A single aperture with subwavelength diameter inside a metallic screen is a key component for nanophotonic applications. Despite the fact that the standard aperture theory [14] has been developed since 60 years, analyzing a nano hole pierced inside a real metallic sheet which cannot be assumed as perfectly conducting turns out to be a difficult task. But due to the interest of the problem, a recent effort succeeded in developing a rigorous electromagnetic theory [15,16] of that diffraction problem. The analysis makes use of a Bessel–Fourier basis to represent the various cylindrical components of the electromagnetic field and reduces Maxwell equations into a first order differential set to integrate. In the case of a cylindrical hole, the integration is made via an eigenvalue technique which leads to short computation time. It is then possible to construct field maps and, more generally to study the field evolution in terms of any parameter in order to extract the physical process which governs the extraordinary transmission.

2. Fringe structure of the transmitted field map

The nano hole under study is illustrated in Fig. 1, which states the notations. The radius R (typically equal to 50 nm) is assumed to be much smaller than the wavelength $\lambda = 500$ nm. The thickness t will be varied between 10 and 500 nm. The device is lighted under normal incidence by a plane wave with vector $\vec{E}$ parallel to the x-axis with a unit amplitude. We first choose $R = 50$ nm and $t = 150$ nm. We consider an observation point M located just below the bottom interface at $z = -1$ nm and calculate the square modulus of the total electric field $|\vec{E}(M)|^2$ when the x and y coordinates of M are varied. Fig. 2(a) shows the global field map, while Fig. 2(b) is a zoom in the central part corresponding to the hole. It is clear that $|\vec{E}|^2$ decreases when x and/or y are increased, but the slope of the surface is not the same in the x- and y-direction. Clearly, the polarization of the incident field introduces an anisotropy. Moreover, the zoom in the central region clearly shows that the maximum of $|\vec{E}|^2$ is not located at $x = y = 0$. A sharp maximum occurs at the point M with $x = 50$ nm and $y = 0$, i.e., on the edge of the metal, while nothing is observed at $y = 50$ nm. This is consistent with the results that we obtained in a previous study [17] and is due to the fact that at the edges of the holes, where the incident electric vector is perpendicular to the metal-air borders, there is a charge accumulation caused by the discontinuity of the induced current [18], which results in a sharp increase of the electric field amplitude (edge effect). Recent experimental results of Degiron (see Fig. 2(a) of [19]) fully confirms the existence of such field enhancement on the aperture boundary perpendicular to the incident polarization direction.

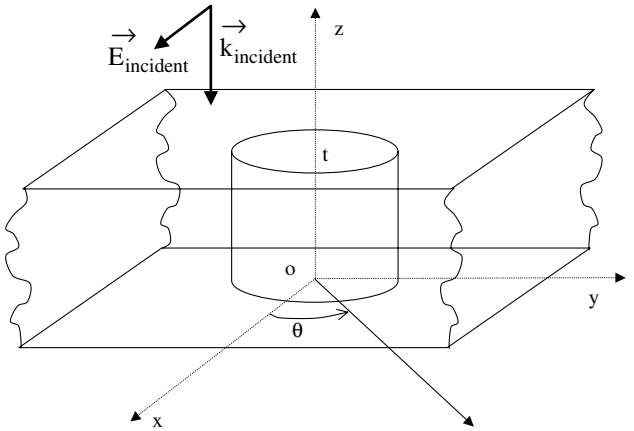

Fig. 1. Illustration of a nanohole inside a metallic screen and notations.

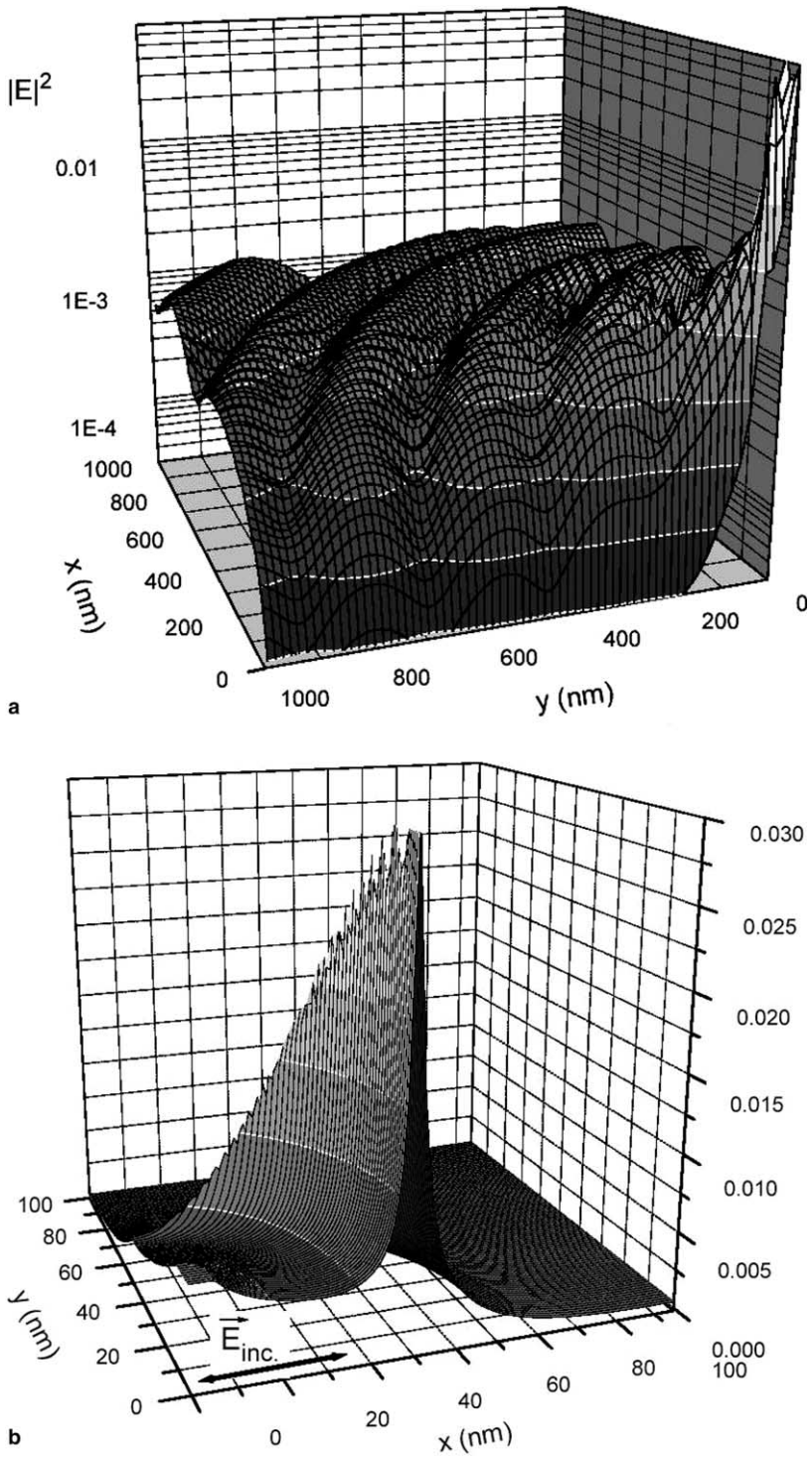

Fig. 2. (a) Square modulus of the electric field map obtained at $z = -1$ nm. (b) Detail of the central region (hole). $R = 50$ nm, $\lambda = 500$ nm, $t = 150$ nm.

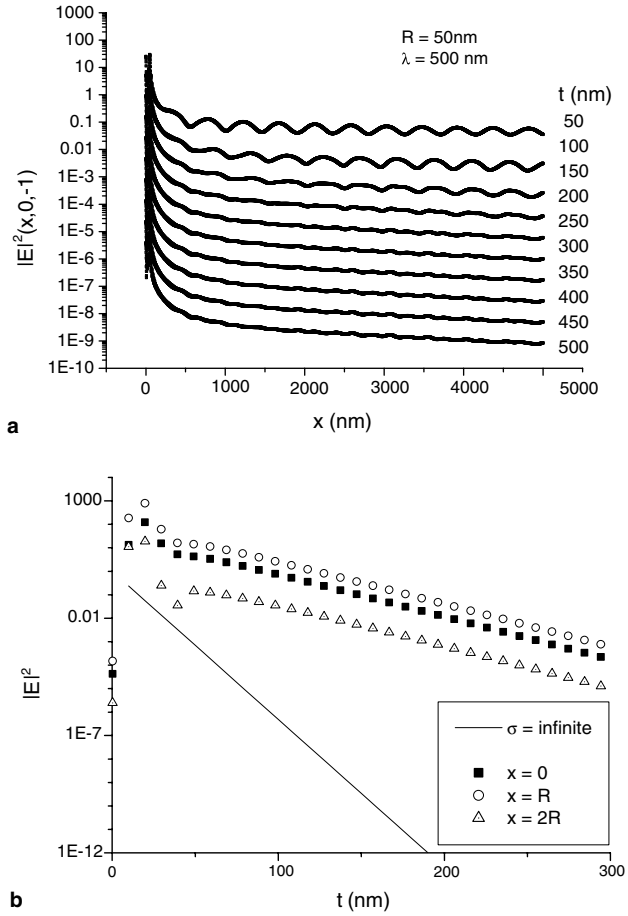

Fig. 3. (a) Variation of the square modulus of the total electric field at a point M just below the bottom interface ($z = -1$ nm) as a function of abscissa x, for various thicknesses of the screen noted in the figure. (b) Variation of $|E|^2$ as a function of t, at a point $M(x, 0, 1\text{ nm})$ for a hole pierced in a perfectly conducting screen (full line) and in a silver screen for three values of x noted in the figure; $R = 50$ nm.

Now, allowing the thickness t to take different values ranging between 50 and 500 nm, we study the evolution of $|\vec{E}(M)|^2$ when the point $M(x, 0, -1)$ is moved parallel to the x-axis. Fig. 3 shows the results. Whatever the thickness t may be, the function $|\vec{E}(x)|^2$ presents a maximum when $x \approx 50$ nm and decays from this value when x is increased. As soon as the thickness t is greater than or equal to 200 nm, the field map remains the same modulo a vertical translation. On the other hand, when t is reduced below 150 nm, a quasiperiodicity in x-direction appears, with an amplitude modulation which increases when t decreases. Of course, the thinner the screen, the larger the mean transmitted square field modulus. This behavior of light diffracted by thin screens pierced by a nanohole has already been predicted by a different theoretical approach using a multiple multipole technique, as shown in Fig. 7(b) of [20]. Our first aim is, by comparing the field map and decay constant with the properties of the mode guided by an infinitely long hollow metallic waveguide, to demonstrate that the transmission through the hole is determined by the behavior of this mode, propagating or evanescent, depending on the hole radius.

The quasiperiodic fringe structure has already been reported in an experimental work [21], and the authors have used a FDTD simulation to

account for their observations. They have concluded that the fringes result from an interference process between a surface plasmon radiated by the hole edge and a wave directly transmitted through the metal film. The second aim of the paper is to confirm this explanation.

In order to address the first point, Fig. 3(b) shows the total electric field intensity as a function of the film thickness at a point $M(x, 0, -1\text{ nm})$ situated immediately below a nano hole with $R = 50$ nm pierced inside a perfectly conducting screen (full line at $x = 0$) and a silver screen. Concerning the perfectly conducting screen, the straight line shows a fast exponential decrease, since the transmitted field may only come from a guided mode inside the nano hole, which is far below the cut-off. In that case, the field has been normalized to unity for $t = 0$. With the finite conductivity, the curves present two different regions. For thickness greater than 100 nm, the field intensity for the three different positions decreases exponentially with a slope much weaker than the one observed with infinite conductivity. This region is discussed in detail in the next section and its properties are due to the existence of an evanescent mode in the hollow metallic waveguide.

For thickness lower than 100 nm, the exponential behavior is first slightly modified, due to the influence of higher order evanescent modes in the nano hole. Then, for $t \leqslant 40$ nm, a more complex behavior occurs, which can be interpreted in the following manner. For $t = 0$, the transmitted field is unity. As soon as a small thickness (10 nm) of silver is introduced, a charge accumulation occurs at top and bottom edge, leading to a field enhancement. But for small t, Coulomb repulsion limits the charge accumulation on the two edges on the side of the hole. This repulsion decreases when t is increased, and we first observe an increase of $|\vec{E}|^2$, with a maximum value for $t = 20$ nm, followed by a decrease due to the exponential decrease of the transmitted field. One can see that, depending on the observation point, the maximum of the field intensity enhancement obtained for $t = 20$ nm ranges between 13 and 900, occurs near the ridge ($x = R$) in agreement with the results presented in Fig. 2.

3. Guided mode inside a nano circular metallic waveguide

In view of explaining the origin of the slow decay shown in Fig. 3(b), we first calculated the effective index γ of the fundamental mode of an infinite metallic circular waveguide made with a perfectly conducting metal or with silver. Fig. 4 shows the real and imaginary part of γ as function of the radius R. For a perfectly conducting metal, a sharp cut-off phenomenon occurs below $R = 146.5$ nm,

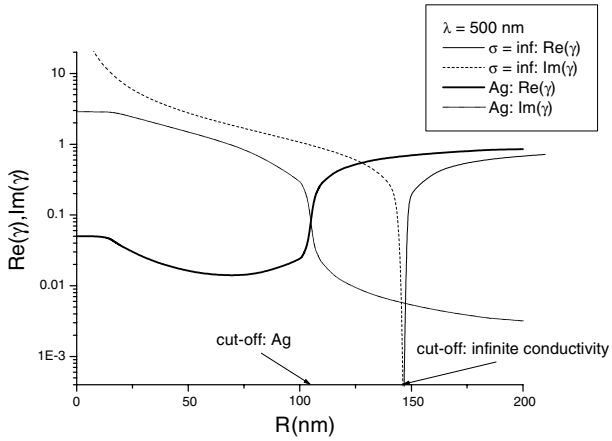

Fig. 4. Real and imaginary part of the propagation constant of the fundamental mode of an infinite circular metallic waveguide made with silver or with a perfectly conducting metal, as function of the radius.

the propagation constant moving from pure real values to pure imaginary ones. The transition is smoother in a real metal like silver, for which a real and an imaginary part always cohabitate. Anyway, below about $R = 103$ nm, the fundamental mode becomes predominantly evanescent. It is worth noticing that the finite conductivity of silver greatly reduces the cut-off radius (the field penetrates in the metallic walls and the effective radius is increased) and that below the cut-off, Im(γ) is always smaller for the silver waveguide than for the perfectly conducting one, which explains the results shown in Fig. 3(b).

Having determined the cut-off radius, close to 100 nm, we plot the transmission factor of a nanohole inside a silver screen, as a function of the thickness, below, on, and above the cut-off radius (Fig. 5). The calculations are done twice, the first time by computing the total field transmitted through the hole, the second time by considering the fundamental waveguide mode only. Above the cut-off, for $R = 125$ nm, the transmission of the single mode as a function of t is almost constant, with a small slope linked with the small imaginary part of γ, close to 10^{-2}. The total field presents small oscillations, due to a Fabry–Perot interference effect produced by the reflection of the propagation field at the top and bottom of the hole. Below the cut-off, the slope of the curves is much steeper and agree with the value of Im(γ) ≈ 1, obtained with $R = 75$ nm in Fig. 4, taking into account the fact that the transmission is proportional to the square of the field. This slope is weaker than the one observed in Fig. 3(b), which is quite natural since in the latter $R = 50$ nm instead of 75 nm, that leads to a higher Im(γ). Of course, for $R = 100$ nm, the slope shows an intermediate steepness, as could be deduced from Fig. 4. For all values of R, the decrease of the total field is governed by the decrease of the fundamental mode, since the slope of the decay of the total field and of the mode is the same when staying below the cut-off. Moreover, the maxima of the small fluctuations observed above the cut-off ($R = 125$ nm) follow the straight line of the corresponding single mode,which is now propagating.

In view of pointing out the link between the guided mode inside the hole and the transmission through the nanohole, Fig. 6 presents the field maps of the modulus of the r, θ and z components of the electric field, for both the fundamental guided mode and for the real total field calculated inside the hole at $z = t/2$. It is evident that the total field inside the hole has the spatial structure of the fundamental guided mode. Moreover, as far as the decay constant of this waveguide mode is always smaller than the attenuation through the film (obtained in Fig. 4 for $R = 0$), the former plays a key role in the extraordinary transmission process (as viewed in Fig. 5).

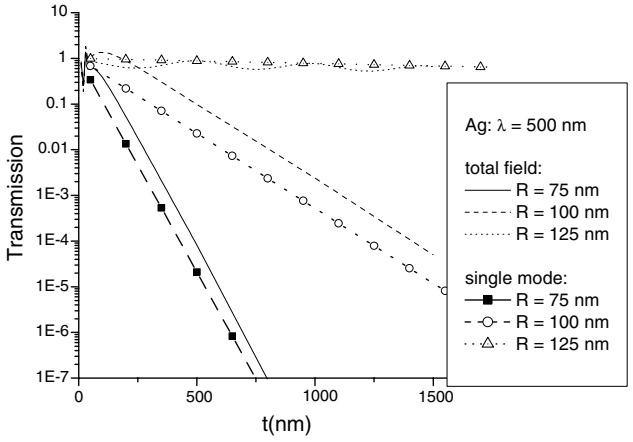

Fig. 5. Transmission of three nanoholes with different radii pierced inside a silver screen as a function of the thickness t.

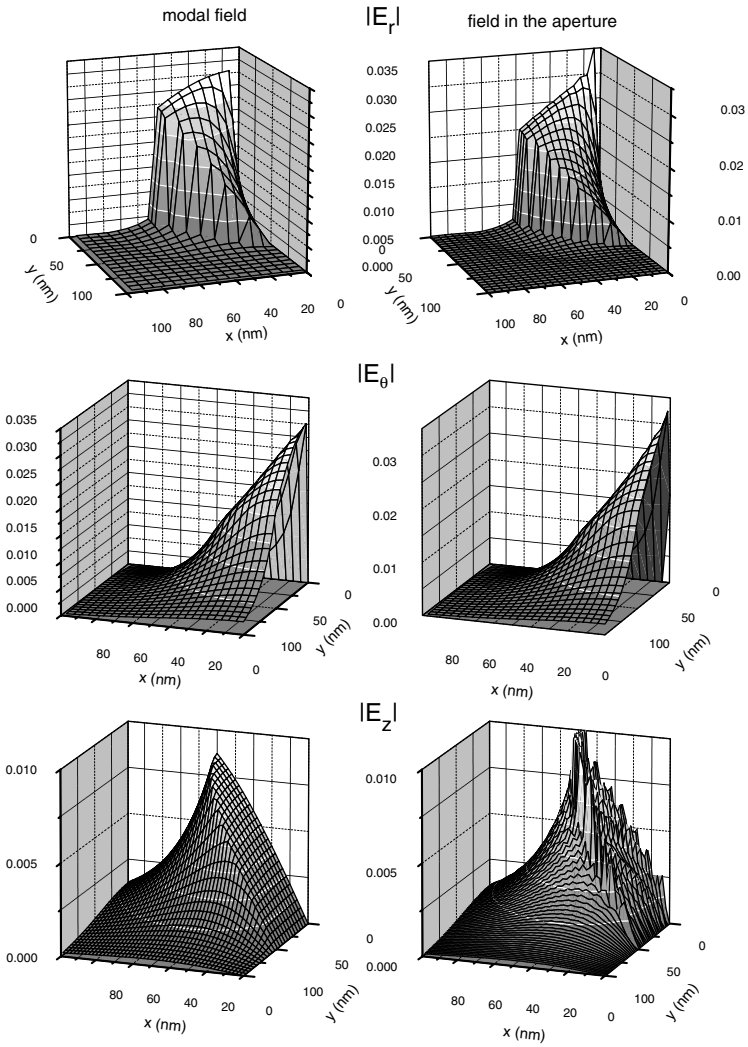

Fig. 6. Maps for the modulus of the components of the electric field for the fundamental guided mode and for the total field in the hole at mid depth.

4. Interference effect

In order to clarify the fringe structure shown in Fig. 3(a), we study separately the x- and z-components of the field. Using the same optogeometrical parameters as in Figs. 3(a), 7(a) and (b) show $|E_x|$ and $|E_z|$ as functions of x for several metal thicknesses. Since the incidence is normal, unpierced silver films will produce a transmitted field with $E_z = 0$, while E_x will be different from zero. Thus, if we follow the explanation developed in [19] and recalled in Section 2, the field maps are expected to be different. Comparison of Fig. 7(a) and (b) confirms these expectations. One observes fluctuations of $|E_x|$ for thinner layers which are absent in $|E_z|$. The relative amplitude of these fluctuations increase with t up to $t \approx 150$ nm and rapidly decreases when $t > 250$ nm.

In addition, one can observe a small variation in their quasiperiod, which becomes shorter for thinner layers. For example, when the thickness is increased from $t = 50$ to 250 nm, the quasiperiod

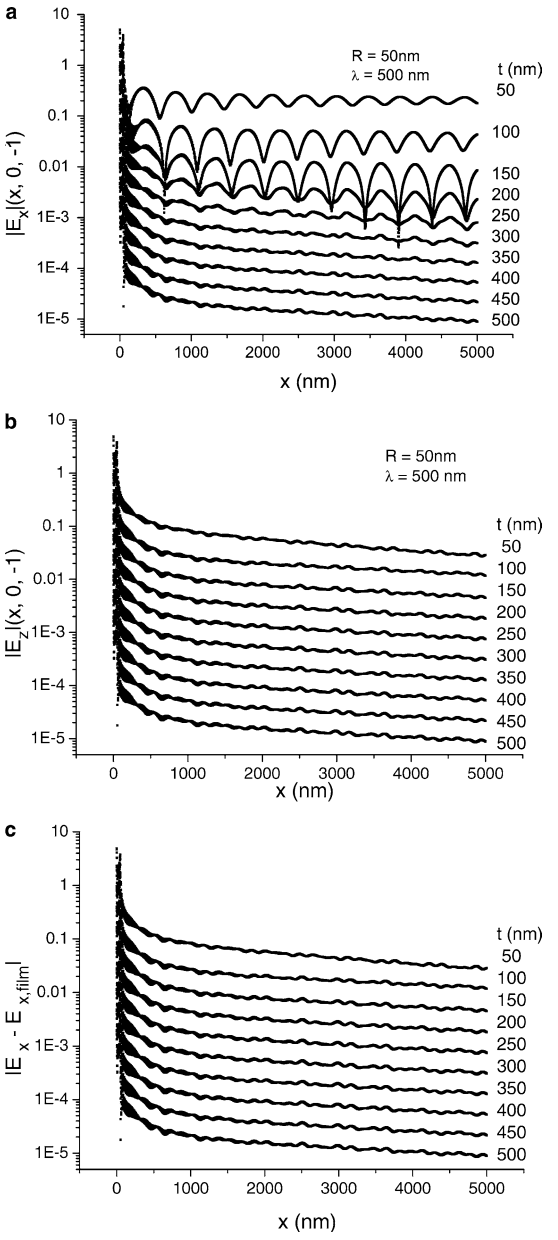

Fig. 7. Field amplitude at a point $M(x,0,1$ nm) below a nanohole in silver screen as a function of x for various thicknesses t (a). $|E_x|$ (b). $|E_z|$ (c). Modulus of the x-component of the field below the nanohole minus the field below the unpierced silver film called $E_{x,\mathrm{film}}$.

d increases from about 450 to 470 nm. This tendency is even more pronounced for thinner layers and is due to the coupling between the plasmons propagating on the two faces of the layer. We devote the next section to its study.

Assuming that a surface plasmon E_p propagating at the bottom interface of a silver film has an x-dependence of the following form [17]:

$$E_{\mathrm{p},x} = \frac{a_x}{\sqrt{x}} \exp\left(\mathrm{i}k_0\alpha'_\mathrm{p}x + \mathrm{i}\varphi_x\right) \exp\left(-k_0\alpha''_\mathrm{p}x\right), \qquad (1)$$

$$E_{\mathrm{p},z} = \frac{a_z}{\sqrt{x}} \exp\left(\mathrm{i}k_0\alpha'_\mathrm{p}x + \mathrm{i}\varphi_z\right) \exp\left(-k_0\alpha''_\mathrm{p}x\right), \qquad (2)$$

where $k_0 = 2\pi/\lambda$, and φ_x and φ_z are phase factors, the phase of the plasmon varies with a x-period d_p related to α'_p by $\alpha'_\mathrm{p} = \frac{\lambda}{d_\mathrm{p}}$. Taking $d = 470$ nm (for $t > 150$ nm) and $\lambda = 500$ nm, we find $\alpha'_\mathrm{p} = 1.064$, which is in excellent agreement with the value of the plasmon propagation constant along air–silver interface. Since the z-component of the transmitted field is null, $|E_z|$ reduces to the modulus of the z-component of the plasmon E_p and no interference effect is seen (Fig. 7(b)). On the other hand (Fig. 7(a)), E_x is the sum of a transmitted field $E_{\mathrm{x\ film}}$ equal to a constant a_1 for $z = \mathrm{const.}$, plus a plasmon field $E_{\mathrm{p},x}$ equal to $(a_x/\sqrt{x})\exp(\mathrm{i}k_0\alpha'_\mathrm{p}x + \mathrm{i}\varphi_x)\exp(-k_0\alpha''_\mathrm{p}x)$. Thus, the square modulus of the sum is modulated with a period $d_\mathrm{p} = \frac{\lambda}{\alpha'_\mathrm{p}} = 470$ nm for large thicknesses. Moreover, when t is increased from 50 nm, a_1 is decreased more rapidly than the field transmitted through the hole, as discussed in detail in the previous section. Thus, the contrast of the interference figure varies with t and depends on the relative strength of a_1 and a_x. When the film thickness is sufficiently large, a_1 becomes negligible compared with a_x and the interference effect disappears. Fig. 3(a) combines the behaviors of Fig. 7(a) and (b). In order to confirm this interpretation, we have plotted in

Table 1
Propagation constant of a plasmon along a silver film for different film thicknesses

t (nm)	α'_p	$\mathrm{Im}(\alpha''_\mathrm{p})$
5	4.0181	0.13233
10	2.203	0.061
15	1.6627	0.03651
20	1.425	0.0245
25	1.30215	0.0177
30	1.22985	0.01346
250	1.0668	0.00257

Fig. 7(c) the modulus of the difference between E_x and the field $E_{x,\mathrm{film}}$ transmitted by the unpierced silver film. No fringes appear and the curves are quite similar to those obtained for $|E_z|$, not only for the shape but also for the amplitudes. The conclusion is that the interference effect suggested by the authors of [19] is fully observed on relatively thin films, not thick enough to completely attenu-

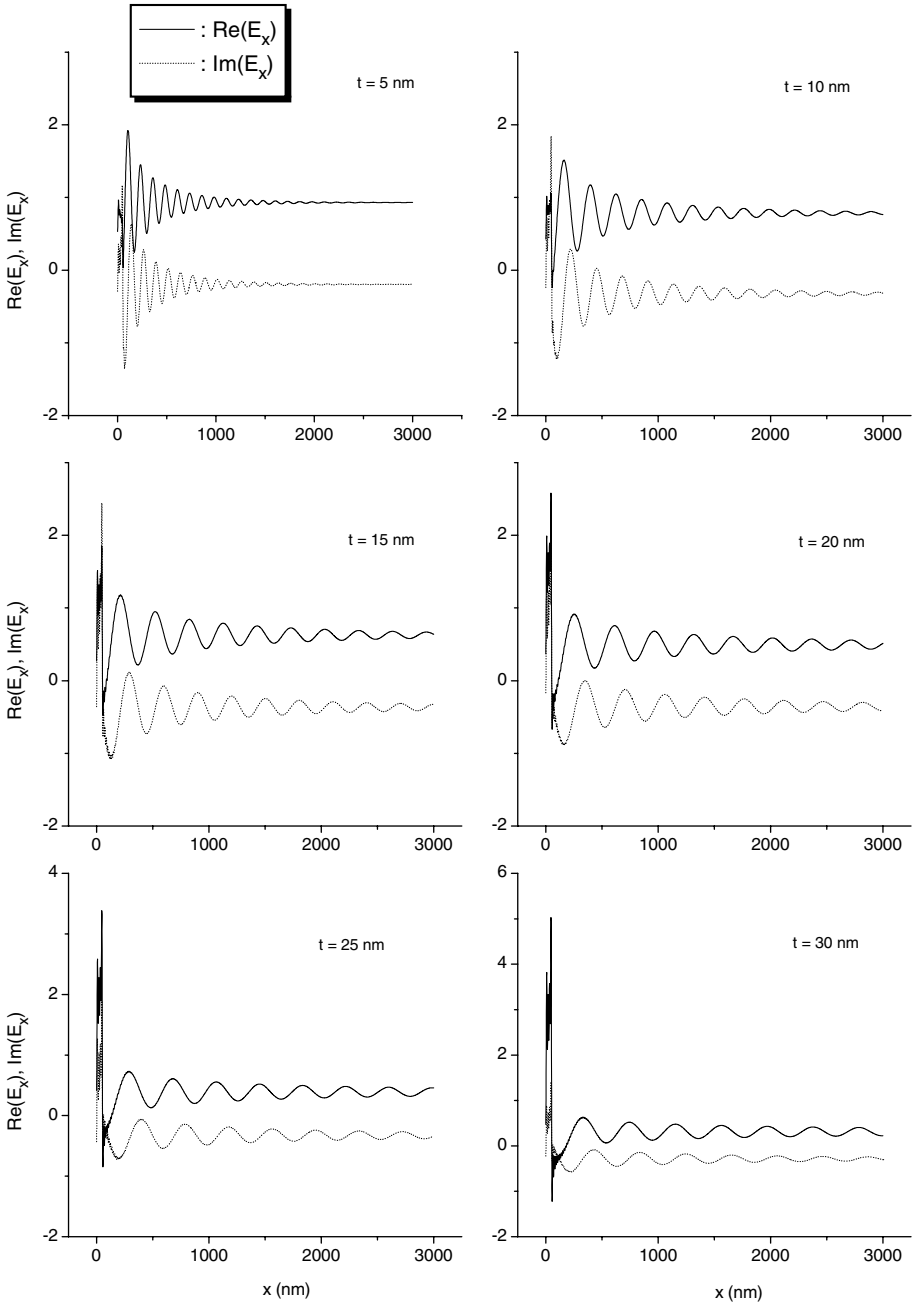

Fig. 8. Variation of $E_x(x)$ for several low thicknesses.

ate the field transmitted through the film when compared to the field transmitted through the aperture.

5. Extremely thin screens

We have observed in Fig. 7(a) that when the thickness t is reduced, the plasmon period reduces. This is due to the increasing coupling between the surface plasmons at the upper and lower interface [10,12]. It greatly modifies the plasmon propagation constant α_p, as is shown in Table 1, which presents α_p for several thicknesses. The result is a reduction of the period of the interference fringes by a factor 3–5, when t is reduced from 40 to 5 nm. Such a reduction is thus expected in the exact numerical results. Using the same optogeometrical parameters, Fig. 8 shows the real and imaginary part of E_x calculated using the electromagnetic

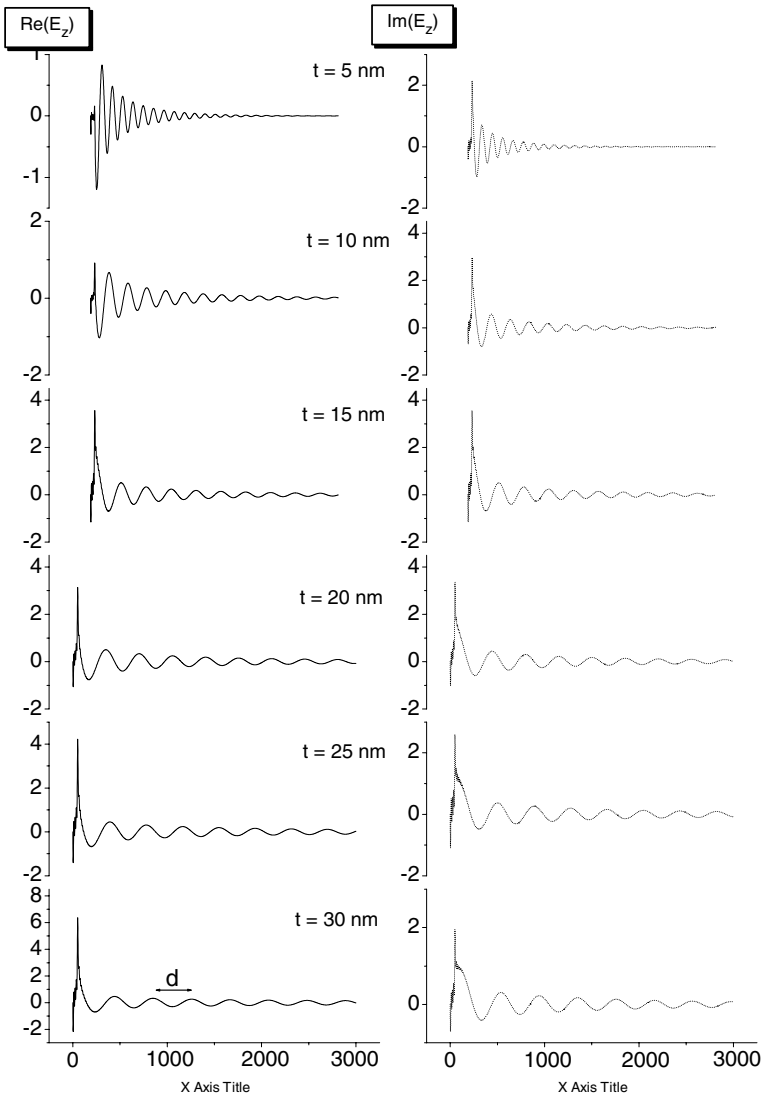

Fig. 9. Variation of $E_z(x)$ for several low thicknesses.

theory [16] as function of x, for different values of t ranging from 5 to 30 nm. Fig. 9 presents the same results for E_z. Comparing Figs. 8 and 9, it is clear that E_x has a non-zero mean value, while for E_z it is not so. This comes from the fact that the device is lighted under normal incidence, so that the z-component of the transmitted field is zero. In all figures, it is seen that the period of the modulations is the same for E_x and E_z and that it increases when t is increased, as can be deduced from Table 1, which establishes the plasmon origin of the phenomenon. Moreover, as expected from the discussion in Section 3, whereas the mean value decreases with t as expected for a transmitted field, the values of $E_x(0)$ and $E_x(R)$ increase with t within this range of its variation. An increase of $E_z(R)$ can also be observed.

The reduction of the plasmon phase period due to coupling phenomena is not limited to thin films. A recent work [22] demonstrates experimentally that a significant shift in the phase period of excited plasmon on a pair of apertures in Au films when the distance between the apertures decreases, due to the coupling between the neighboring localized surface plasmons.

6. Conclusion

The extraordinary light transmission through nano holes is linked with the finite conductivity of the screen which produces lower attenuation for guided modes below the cut-off than in the case of infinite conductivity. In addition, the finite conductivity allows for surface plasmon excitation, which field dominates the near-field distribution in the very vicinity below the film. The numerical results obtained using a rigorous electromagnetic analysis can be fully explained using the concepts of leaky guided mode inside the hole, and surface plasmon at the bottom interface, the latter being, eventually, modified by coupling with the upper interface plasmon when the thickness of the screen is small. For thicknesses at which the transmitted field through the layer is non-negligible, a fringe structure of the field map exists for some field components, due to interference with the surface plasmon field.

References

[1] T.W. Ebbesen, H.J. Lezec, H.F. Ghaemi, T. Thio, P.A. Wolff, Nature 391 (1998) 667.
[2] U. Schröter, D. Heitmann, Phys. Rev. B 58 (15) (1998) 419.
[3] M.M.J. Treacy, Appl. Phys. Lett. 75 (1999) 606.
[4] J.A. Porto, F.T. Garcia-Vidal, J.B. Pendry, Phys. Rev. Lett. 83 (1999) 2845.
[5] H.F. Ghaemi, T. Thio, D.E. Grupp, T.W. Ebbesen, H.J. Lezec, Phys. Rev. B 58 (1998) 6779.
[6] E. Popov, M. Nevière, S. Enoch, R. Reinisch, Phys. Rev. B 63 (2000) 16100.
[7] S. Enoch, E. Popov, M. Nevière, R. Reinisch, J. Opt. A 4 (2002) S83.
[8] A. Krishnan, T. Thio, T.J. Kim, H.J. Lezec, T.W. Ebbesen, P.A. Wolff, J.B. Pendry, L. Martin-Moreno, F.J. Garcia-Vidal, Opt. Commun. 200 (2001) 1.
[9] L. Martin-Moreno, F.J. Garcia Vidal, H.J. Lezec, K.M. Pellerin, T. Thio, J.B. Pendry, T.W. Ebbesen, Phys. Rev. Lett. 86 (2001) 1114.
[10] S.A. Darmanyan, A.V. Zayats, Phys. Rev. B 67 (2003) 035424.
[11] N. Bonod, S. Enoch, L. Li, E. Popov, M. Nevière, Opt. Express 11 (2003) 483.
[12] S. Darmanyan, M. Nevière, A.V. Zayats, Phys. Rev. B 70 (2004) 075103-1.
[13] S. Darmanyan, M. Nevière, A.V. Zayats, in: F. Abdullaev, V. Konotop (Eds.), Nonlinear Waves: Classical and Quantum Aspects, NATO Science Series: Mathematics, Physics and Chemistry, vol. 153, Kluwer Academic Publishers, Dordrecht, 2004, p. 313.
[14] H.A. Bethe, Phys. Rev. 66 (1944) 163.
[15] N. Bonod, E. Popov, M. Nevière, Opt. Commun. 245 (2005) 355.
[16] N. Bonod, E. Popov, M. Nevière, J. Opt. Soc. Am. A 22 (2005) 481.
[17] E. Popov, N. Bonod, M. Nevière, H. Rigneault, P.F. Lenne, P. Chaumet, Appl. Opt. 12 (2005) 2332.
[18] R. Zakharian, M. Mansuripur, J.V. Moloney, Opt. Express 12 (2004) 2631.
[19] A. Degiron, H.J. Lezec, N. Yamamoto, T.N. Ebbesen, Opt. Commun. 239 (2004) 61.
[20] R. Wannemacher, Opt. Commun. 195 (2001) 107.
[21] L. Yin, V.K. Vlasko-Vlasov, A. Rydh, J. Pearson, U. Welp, S.H. Chang, S.K. Gray, G.C. Schutz, D.B. Brown, C.W. Kimball, Appl. Phys. Lett. 85 (2004) 467.
[22] J. Prikulis, P. Hanarp, L. Olofson, D. Sutherland, M. Käll, Nano Lett. 4 (2004) 1003.